Int. J. Electrochem. Sci., 8 **(2013)** 3615 - 3627

International Journal of
ELECTROCHEMICAL
SCIENCE
www.electrochemsci.org

Electrocatalytic Properties of Electroless NiP- RuO_2/TiO_2 Composite Coatings

Jelica Novakovic, Panayota Vassiliou and Elsa Georgiza

School of Chemical Engineering, National Technical University of Athens, 9, Iroon Polytechniou Str, GR- 157 73 Zografou, Athens, Greece
*E-mail: jelica@central.ntua.gr

Received: 18 January 2013 / *Accepted:* 2 February 2013 / *Published:* 1 March 2013

Composite NiP-RuO_2/TiO_2 coatings were deposited by simultaneous electroless codeposition of Ni-P metal matrix and mixtures of RuO_2/TiO_2 oxides on steel and brass substrates from a reducing solution in which particles were kept in suspension by stirring. Mixed oxides RuO_2/TiO_2 were prepared by thermal decomposition in air of a $RuCl_3/TiO_2$ suspension at 450 ^oC. Deposits were characterized by means of X-ray diffraction, scanning electron microscopy SEM, EDX and cyclic voltammetry. The obtained composite coatings exhibit the same morphology on both types of substrates. The electrocatalytic activity of the layers for hydrogen evolution reaction in 1M NaOH alkaline solution was determined by linear sweep technique with a slow sweep rate (ν = 0.2 mV/s). Polarization curves recorded on mixed oxide reinforced Ni-P electrodes show a unique Tafel slope of approximately 120mV/dec in the whole potential range (–1.1/-1.5 V vs. SCE), while polarization curves obtained on NiP-RuO_2 composite coatings are bent with Tafel slopes of about 90 mV/dec at low current densities and 200 mV/dec at higher current densities. NiP-RuO_2/TiO_2 electrode activity increases with RuO_2, thus NiP-RuO_2 electrode showing the highest activities on both types of substrates.

Keywords: Electroless Ni-P, Composite coatings, mixed RuO_2/TiO_2 oxide, Hydrogen evolution reaction, Electrocatalysis

1. INTRODUCTION

Transition metal oxides embedded in a metallic matrix can lead to the production of electrode materials which interest the chlor-alkali industry because of their good electrocatalytic properties for the chlorine evolution reaction [1-4]. Some of the transition metal oxides are also active for the hydrogen evolution reaction (HER) [1, 3, 5-7]. High electrocatalytic activity for ZrO_2, RuO_2, IrO_2, and TiO_2 reinforced electroless Ni-P coatings has been reported [8-11].

Dimensionally Stable Anodes (DSA) electrodes, born for chlorine evolution have also shown their activity for almost all other more common electrocatalytic reactions such as O_2 evolution, O_2

reduction, H_2 evolution (although in the latter case the conditions are even against thermodynamics), as well as organic oxidation. The reason for activity has been identified in the surface redox reactions taking place at transition metal ions acting as active sites [12, 13]. These redox centers, coupled with the moderate interaction of intermediates with the oxide surface precisely due to the particular structure of oxides, are able to catalyze a variety of electrode reactions in a potential range close to that of the surface redox couple [14].

The major components of DSA are RuO_2, which imparts its high electrocatalytic activity, and TiO_2, which brings its chemical inertness. Use of the mixed oxide - noble metal oxide with TiO_2 makes the process of composite incorporation for the improved electrocatalytic activity less costly, without any reduction in the electrocatalytic activity, than when pure noble metal oxide is used [15]. If these materials can couple the electrochemical activity of the dispersed phase to the electrical conductance, mechanical and chemical stability of the matrices, they may be of practical interest since they contain reduced amounts of the often-expensive electrocatalytic species.

In this work, mixed oxide of RuO_2 with less expensive TiO_2 support is used as the composite for improving the electrocatalytic activity of electroless NiP coating for hydrogen evolution reaction.

2. EXPERIMENTAL

2.1 Electroless plating

Carbon steel and brass flat cylindrical specimens with diameter of 25 mm and 13 mm height were employed as substrate. All coatings were deposited on smooth steel and brass substrate. The samples were polished to 1000 grit then cleaned in an alkaline solution, for 5 min. in an ultrasonic bath, followed by water rinse. Before the deposition the steel samples surface is activated by dipping in a 15% HCl aqueous solution for 5 minutes. The brass specimens were activated in a 20 % HNO_3 and at first they were electrolytically flush nickel plated in a bath with the following composition: [$NiSO_4(NH_4)_2SO_4$ x $6H_2O$)] 25 g/l $NiSO_4x7H_2O$ 100 g/l, NH_4Cl 20 g/l and H_3BO_3 20 g/l with anodes of nickel and a current density of 1 A/dm^2, at room temperature.

Table 1. Plating solution and deposition conditions

	Ni-P [g/l]	Ni-P- RuO_2/TiO_2, Ni-P- RuO_2 [g/l]
$NiSO_4$ x $6H_2O$	21	21
NaH_2PO_2 x H_2O	24	24
Lactic acid	28	28
Propionic acid	3	3
RuO_2/TiO_2, RuO_2	-	2, 0.5
Pb^{2+} [ppm]	0.5-1.0	0.5-1.0
pH	4.4-4.7	4.4-4.7
Temperature	95 ± 1 ^oC	95 ± 1 ^oC

The RuO_2/TiO_2 mixed oxides were prepared by thermal decomposition method. At first TiO_2 powder (200-300 nm) was soaked in isopropanol solution containing $RuCl_3$. The solvent was slowly evaporated and the dry mass was heated at 250^{o}C for one hour in an oven. It was powdered finely using a mortar and then fired at 450^{o}C in a furnace for another hour in order to complete conversion of $RuCl_3$ to RuO_2. Oxides with 10, 20 and 30% of RuO_2 were prepared.

The bath composition and conditions are shown in Table 1.

Nickel sulfate is the nickel source sodium hypophosphite is the reducing agent, lactic and propionic acids act as complexing and buffering agents and lead act as a bath stabilizer.

The oxide powder was added to the plating solution and stirred with a magnetic stirrer for 24 hours at room temperature in order to obtain a better wettability. The suspension was next ultrasonicated for 10 minutes to decrease particles agglomeration and heated to 95 ± 1^{o}C prior to deposition. The bath is stirred by a stirrer at 500 rev/min and the deposition process has been carried out for 2 h at constant temperature.

NiP-RuO_2/TiO_2 and NiP-RuO_2 composite coatings were produced with 2.0 and 0.5 g/l particles bath load, respectively. It should be noticed that in the case of NiP-RuO_2 nonuniform deposits were produced and after 1.5 hours of codeposition there was a tendency for bath decomposition. NiP-RuO_2/TiO_2 composite coatings were uniformly deposited and the bath was stable during 2 hour codeposition, which is attributed to chemical inertness of TiO_2 particles.

2.2 Physico-chemical characterization

The microhardness of the substrate and of the coatings was measured using a Leitz Wetzlar tester with a Vickers diamond indenter. Measurements were carried out on the specimen surface employing a load of 100 g for a period of 10s. An average of seven measurements was reported as the microhardness value.

The surface morphology of both Ni-P and NiP-RuO_2/TiO_2 layers was examined by means of scanning electron microscopy equipped with EDS analysis, which was used for the determination of chemical composition of the deposits. X-ray diffraction analysis has been also performed using a Cu K_α x-ray source (SIEMENS X-ray Diffractometer 5000) to study the structural changes in the produced coatings. A Talysurf instrument was employed to provide roughness data over an 8 mm length of the test specimen. Eight replicate scans were performed.

2.3 Electrochemical characterization

The $E - i$ polarization curve of the composite electroless Ni-P-RuO_2/TiO_2 in 1M NaOH were obtained at room temperature by the linear sweep technique at a slow sweep rate ν = 0.2 mV/s going in the negative direction from -1.07 to -1.5 V vs. saturated calomel electrode (SCE) as reference electrode. The working electrodes were placed in a Teflon sample holder and the surface was masked so that the geometric area was set to 0.28 cm^2 and the electrode surface was vertically placed into the electrolyte to facilitate H_2 bubbles detachment. A Pt wire of ca. 8 cm^2 inside a glass tube was used as

counter electrode separated from the electrolyte by a porous fritted glass diaphragm. Prior to each experiment the electrode surface was cleaned and reduced at -1.5 V for 5 min then left at open circuit potential for another 5 min.

The instrumentation was a CMS 100 Gamry potentiostat, computer controlled with automatic correction of the IR drop and commercial software for the obtained data treatment.

3. RESULTS AND DISCUSSION

3.1 Characteristics of the deposits

The RuO_2/TiO_2 mixed oxides were prepared by thermal decomposition. The conversion of $RuCl_3$ to RuO_2 was confirmed by XRD analysis. RuO_2 and TiO_2 particles had crystalline structure of rutile and anatase respectively. The X-ray diffractograms of the prepared mixed oxides are shown in Fig. 1. It can be observed that RuO_2 diffraction peaks increase as its concentration increase in the formed mixed oxide.

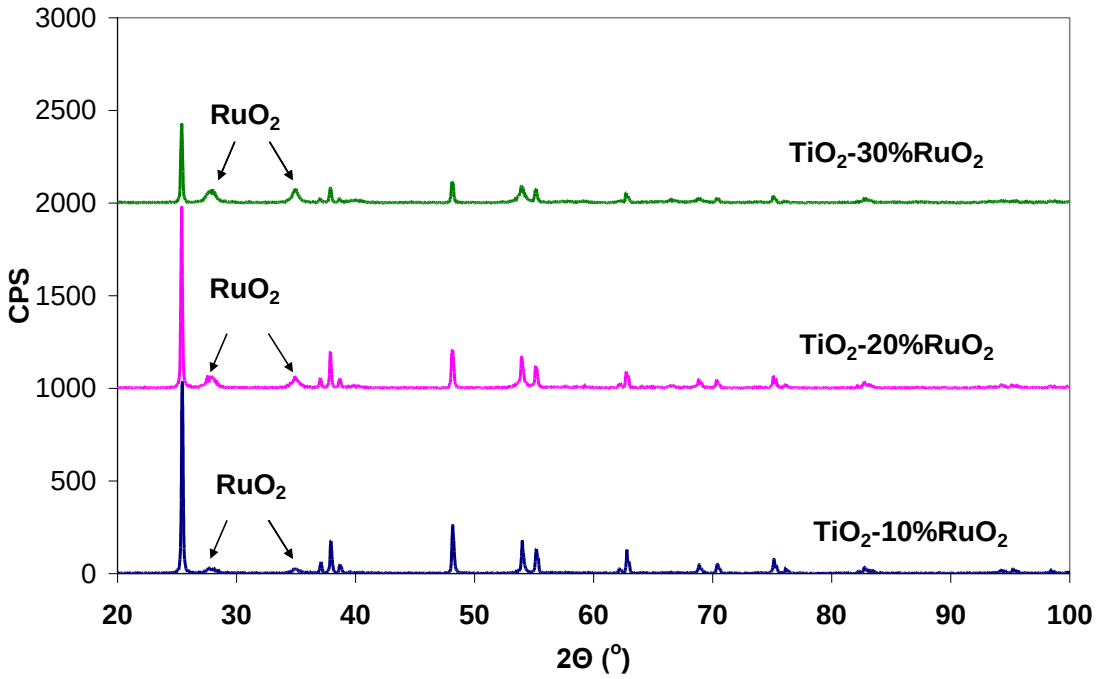

Figure 1. XRD patterns of the prepared RuO_2/TiO_2 mixed oxides

The chemical compositions of the as-plated Ni-P and composite Ni-P-RuO_2/TiO_2 coatings obtained by EDS analysis are presented in Table 2. High phosphorous coatings with high particle incorporation are obtained on both types of substrates. Observed Ti/Ru ration is approximately 1.5 fold lower than expected. This may indicate the surface enrichment of noble RuO_2 oxide, which is normal in mixed oxides as the affinity for oxygen differs among the components [15].

Table 2. Composition of the Ni-P and NiP-RuO_2/TiO_2 composite coatings on steel and brass substrate in relation to mixed oxide RuO_2 concentration by EDS

Deposit Composition. wt.%						
Steel Substrate						
RuO_2. %	Ni	P	Ru	Ti	Ti/Ru*	Ti/Ru**
10	80.2	14.5	1.0	4.3	4.3	7.1
20	79.8	15.4	1.5	3.2	2.1	3.2
30	80.6	14.3	2.3	2.8	1.2	1.8
100	80.3	13.6	6.0	0	0	
Brass Substrate						
	Ni	P	Ru	Ti		
10	80.6	13.8	1.0	4.5	4.5	7.1
20	79.5	14.8	1.9	3.7	1.9	3.2
30	78.9	14.7	3.0	3.4	1.1	1.8
100	79.8	13.8	6.3	0	0	
Ti/Ru*- experimental ratio. Ti/Ru**- theoretical ratio						

Scanning electron microscope images show considerable differences in the appearance of the surface of the plain Ni-P coatings on steel and brass substrate. The Ni-P coatings on steel substrate are fine grained (Fig. 2) with apparent nodule formation. Most of the grains are from 2-5 μm, whereas on the brass substrate much larger grains: mostly 10 – 35 μm are observed.

Figure 3 shows representative surface morphologies of the as-plated NiP-RuO_2/TiO_2 and NiP-RuO_2 composite deposits with different RuO_2 concentrations on the brass substrate.

Mixed oxide incorporated coatings show the same, matt, dark grey, velvet like structure on both type of substrates (steel and brass). It looks like that the particles were incorporated and attached to the metal matrix in the form of small cluster chains (Fig. 3). NiP-RuO_2 composite coatings show similar but more developed structure.

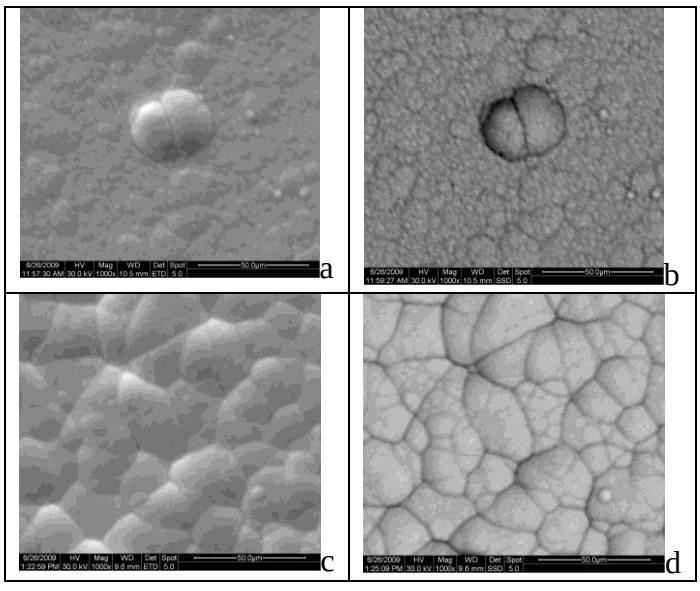

Figure 2. Surface morphology (SE and BS images) of the plain Ni-P coatings on steel (a, b) and brass (c, d) substrate and

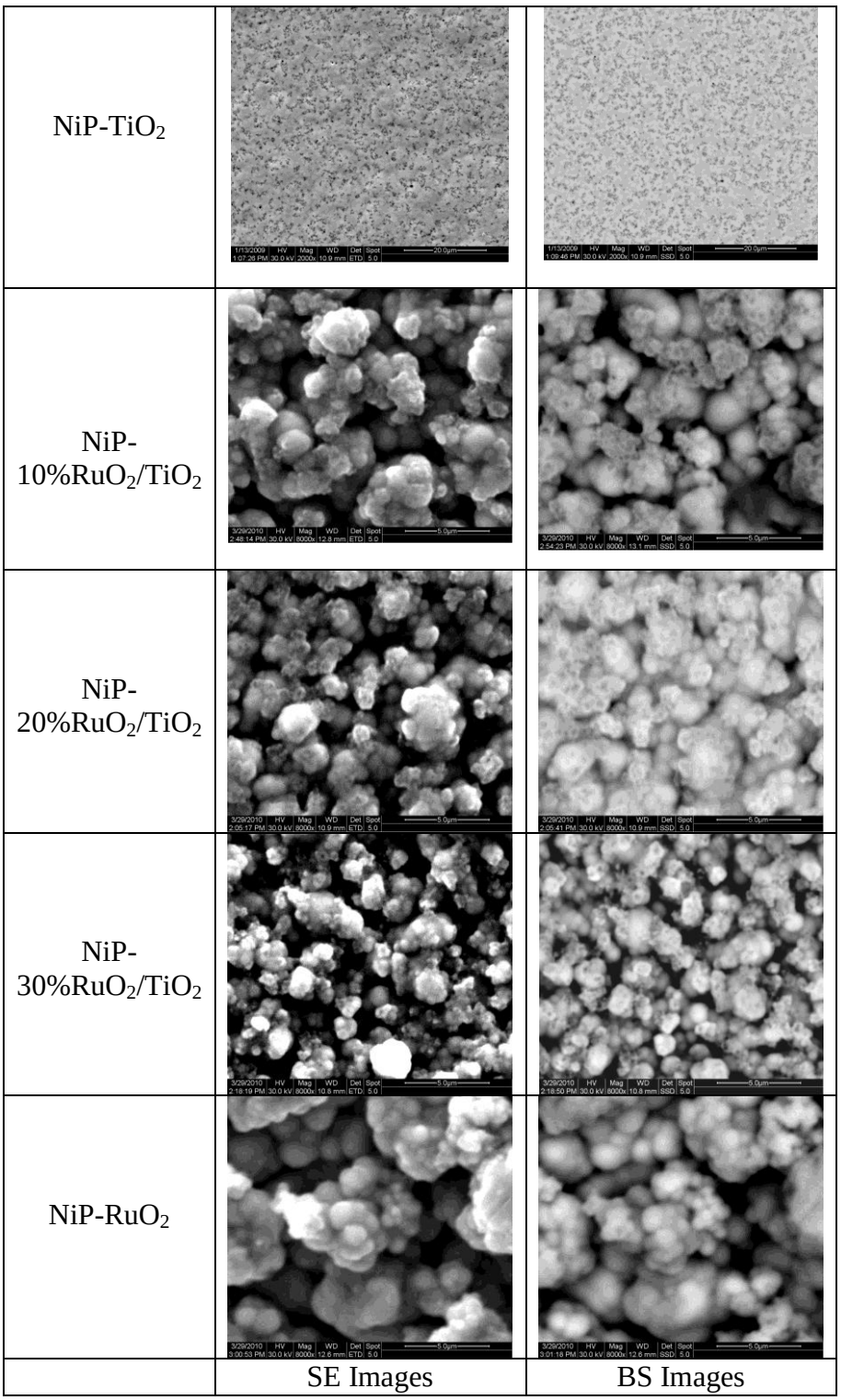

Figure 3. Surface morphology (SE and BS images) of the as-plated NiP-TiO_2, NiP-RuO_2/TiO_2 composite deposits with different RuO_2 concentrations and NiP-RuO_2 on the brass substrate

Table 3 summarizes microhardness values of the as-plated NiP-RuO_2/TiO_2 composite deposits with different RuO_2/ TiO_2 concentrations on both substrates. The microhardness of the mixed oxide reinforced NiP deposits shows lower values than that of NiP-TiO_2 deposits [16], which may be

indicative of weaker particle-matrix interactions. This fact, as well as deposit morphology could also signify a different way of particles incorporation. During plating process, the reducing agent is oxidized, and the Ni^{2+} ions are reduced on the activated substrate. The Ni, once deposited, acts as a catalyst for further deposition of Ni. In the case of NiP-TiO_2 coatings, TiO_2 particle dispersed by stirring the bath, seem to be physically entrapped in the growing layer of NiP plating (Fig.3). Mixed oxides NiP-RuO_2/TiO_2, as well as, NiP-RuO_2 composite coatings give the impression that the particles dispersed in solution were acting as catalytic substrate for Ni^{2+} reduction consequently forming small clusters which then were embedded into the matrix. Bonding between the clusters seems not to be too strong, thus giving rise to lower microhardness values.

Table 3. Microhardness of the Ni-P, NiP-TiO_2 and NiP-RuO_2/TiO_2 composite coatings on steel and brass substrate in relation to RuO_2 concentrations

Microhardness, HV			
RuO_2, %	TiO_2, %	Steel substrate	Brass substrate
0	0	721±12	701±25
0	100	792±25	780±32
10	90	642±85	668±47
20	80	703±89	677±82
30	70	655±55	639±68
100	0	583±53	587±85

In Fig. 4 the X-ray a typical diffraction pattern of the as-plated NiP-RuO_2/TiO_2 composite coatings is presented. No difference was observed on the two types of substrates. The typical diffractogram for the amorphous NiP coating is obtained and the presence of the TiO_2 anatase and rutile RuO_2 peaks can be observed.

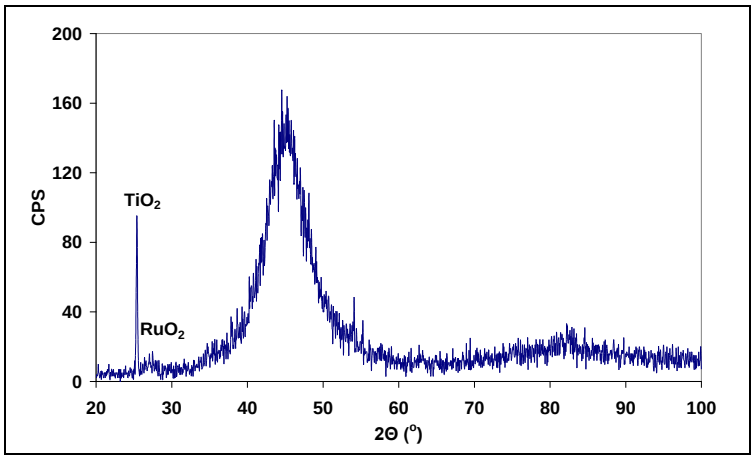

Figure 4. Typical XRD pattern of the as-plated NiP-RuO_2/TiO_2 composite coating

3.2 Electrocatalytic Characteristcs

One of the aims of electrocatalysis is to improve electrode stability by mixing two or more components searching for synergetic effects. The latter are normally attained by as the components come into intimate electronic contact. The study of oxide/solution interfaces establishes interplay between electrocatalysis and surface and colloid chemistry, which highlights new conceptual routes. Surface charging is a completely different mechanism with oxides with respect to metal/solution interfaces [17]. Therefore ionic and non-ionic adsorption is governed by different factors which may lead to different mechanistic routes of electrode processes.

Polarization curve for hydrogen evolution in 1 M NaOH solution are given in Figure 5. No impact of substrate material was observed – the polarization curves behave similarly on both types of substrate steel and brass. For comparison reason apart from polarization curves on the mixed oxide NiP-RuO_2/TiO_2 composite coatings, polarization curve on NiP-TiO_2, NiP-RuO_2 and NiP are also shown. Curves recorded on mixed oxide reinforced NiP electrode show a unique Tafel slope of approximately 120 mV/dec in the almost whole investigated potential range (-1.1 ~ -1.5 V vs. SCE) with increased activity with increasing RuO_2 concentration. Polarization curves obtained on NiP-RuO_2 composite coatings are bent with Tafel slopes of about 90 mV/dec at low current densities (region I) and 200 mV/dec at higher current densities (region II). The curvature of the polarization curve can be explained by a bend towards a limiting current density at higher overpotenatials or by a change in the reaction mechanism. Similar behaviour was observed on commercial DSA (Dimensionally Stable Anodes) electrodes with RuO_2 as the active compound [18].

Shibli et al. reported [8] for the mixed oxide NiP-RuO_2/TiO_2 composite coatings Tafel slope of 33mV/dec. The deviation between our results and theirs is most probably due to differences in the coatings preparation – different electroless NiP bath were used, as well as, due to almost ten fold smaller TiO_2 particles size (~ 30 nm) they utilized.

Kinetic parameters: Tafel slope $\boldsymbol{b}$, exchange current density - $\boldsymbol{i_0}$, and hydrogen overpotential at current density 100 mA/cm^2 - η_{100} are presented in Table 4. The parameters were calculated taking into account the layer geometric surface area.

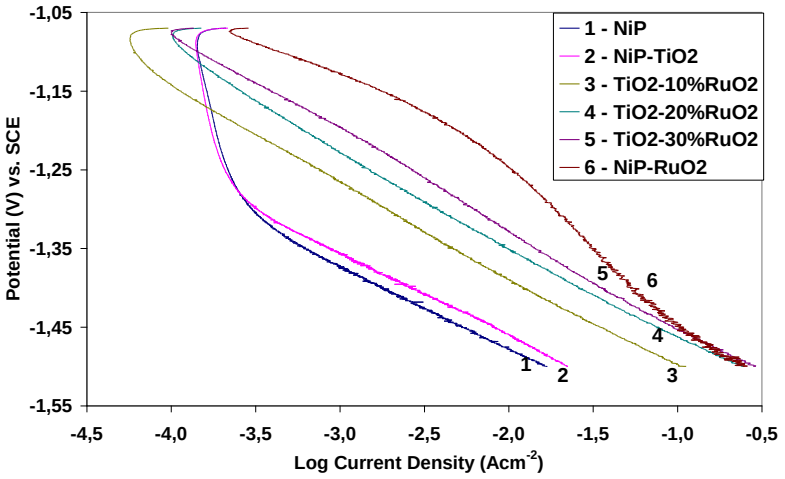

(a)

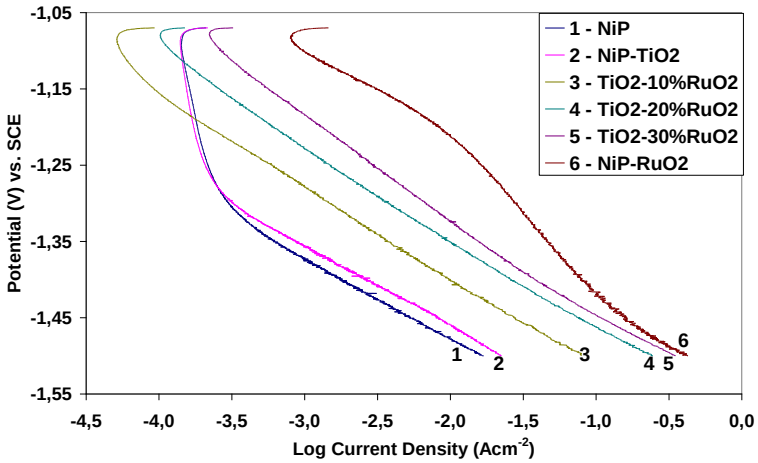

(b)

Figure 5. Linear polarization curves of the plain Ni-P and composite NiP-RuO_2/TiO_2 NiP-TiO_2 and NiP-RuO_2 deposits on steel (a) and brass substrate (b)

Table 4. HER kinetic parameters obtained from the Tafel curves of the plain Ni-P and composite NiP-RuO_2/TiO_2 NiP-TiO_2 and NiP-RuO_2 deposits on steel and brass substrate in 1M NaOH solution at 298 K

Kinetic parameters of the HER							
Electrode		Steel substrate			Brass substrate		
		b_C mV/dec	i_o μA/cm^2	η_{100} mV	b_C mV/dec	i_o μA/cm^2	η_{100} mV
0	0	-118.2	2.11	553	-118.2	2.11	553
0	100	-105.8	2.02	497	-105.8	2.02	497
10	90	120.7	23.98	316	120.2	18.57	328
20	80	-123.3	34.75	302	-125.2	57.51	280
30	70	-126.0	91.43	257	-131.7	132.3	247
100^{I}	0	-96.9	231.4	158	-81.5	267.4	128
100^{II}	0	-194.7	1195	180	-199.1	2250	129
Region I: – 1.0 7/-1.2 V; Region II -1.2/-1.5 V vs. SCE							

Figure 6 shows that at the constant electrode potential (-1.4 V vs. SCE) the reaction rate on composite NiP-RuO_2/TiO_2 and NiP-RuO_2 is approximately 8-30 times faster than on the plain Ni-P and NiP-TiO_2 composite electrode materials. NiP-RuO_2/TiO_2 electrode activity increases with RuO_2 content increase, thus NiP-RuO_2 electrode showing the highest activities on both types of substrates. Also, higher exchange current densities and significantly lower overpotentials at current density of 100mA/cm^2 have been observed on NiP-RuO_2/TiO_2 and NiP-RuO_2 composite electrodes (Tab. 4).

Porosity is a typical feature of oxide electrodes related to the specific procedure of preparation. Porosity measures the fraction of surface which is less accessible to the reacting particles (inner surface) [19, 20]. Usually, the inner surface is excluded from the reaction after a few initial moments.

This is what happens in case of chlorine evolution but it does not for O_2 as well as H_2 evolution. The reason is to be sought in the particular nature of oxide/solution interfaces in aqueous solution [17].

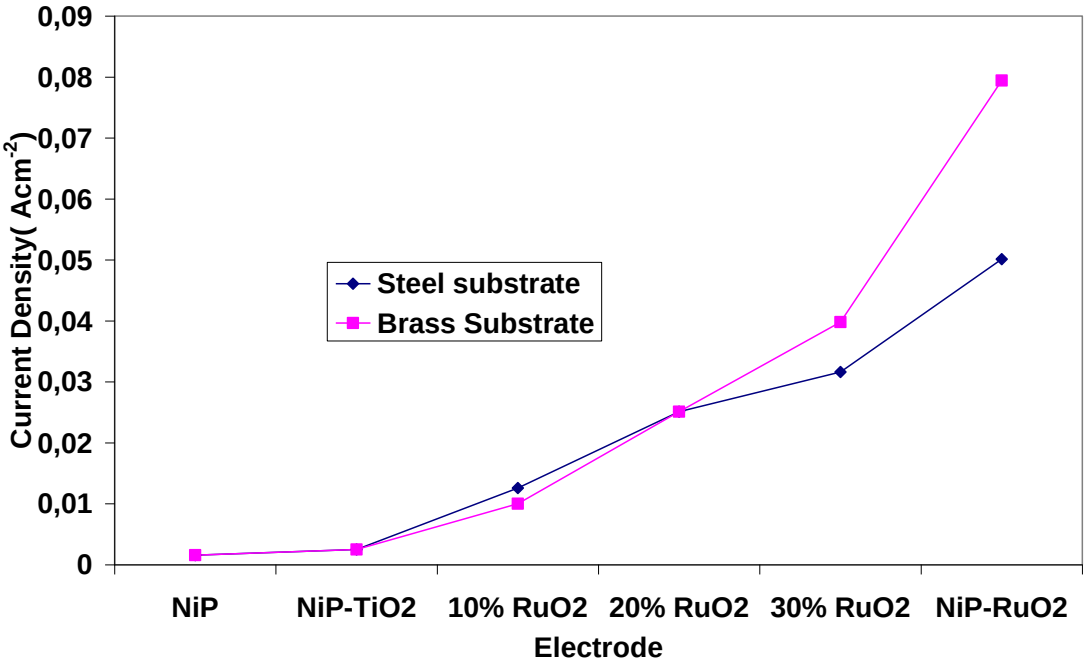

Figure 6. Current Density for hydrogen evolution on the plain Ni-P and composite NiP-RuO_2/TiO_2 NiP-TiO_2 and NiP-RuO_2 deposits on steel and brass substrate

Cyclic voltammetry to obtain q^*, the voltammetric charge, was conducted between -1.3 and 0.2 V vs. SCE at 20 mV/s in 1M NaOH in order to estimate the real electrode surface area. Voltammetric curves were recorded before and after cathodic polarization. The voltammetric charge obtained by integration of the curves measures the amount of protons exchanged with the solution:

$$RuO_2 + \delta H^+ + \delta e^- \leftrightarrow RuO_{2-\delta}(OH)_\delta$$

Such a charge has been pointed out to be proportional to the surface concentration of active sites, hence to the actual surface area [21]. Figure 7 collates the voltammetric curves of the plain Ni-P and composite NiP-RuO_2/TiO_2 layers.

Table 5 shows voltammetric charges, q^* measured for Ni-P and composite NiP-RuO_2/TiO_2 layers on steel (a) and brass (b) substrate in 1M NaOH aqueous solution. It could be seen that q^* values increase with RuO_2 concentration increase and also that they are increased after cathodic hydrogen discharge. This suggests that the active surface has probably grown as a consequence of the solution spreading over regions made hydrophilic by the reductive treatment.

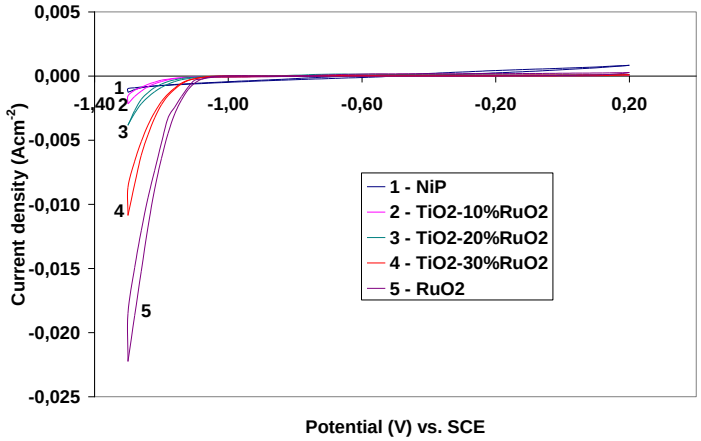

(a)

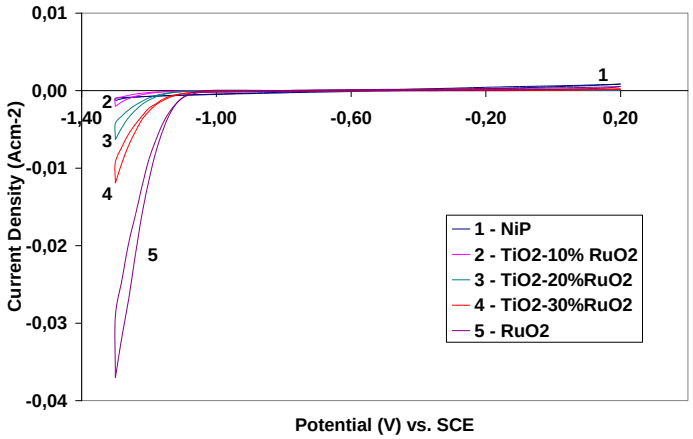

(b)

Figure 7. Representative voltammetric curves (20 mV/s) recorded on Ni-P and composite NiP-RuO_2/TiO_2 layers on steel (a) and brass (b) substrate in 1M NaOH aqueous solution

Table 5. Voltammetric charges recorded on Ni-P and composite NiP-RuO_2/TiO_2 layers on steel (a) and brass (b) substrate in 1M NaOH aqueous solution

Electrode		Voltammetric charge q^*, mC/cm^2	
RuO_2, %	TiO_2, %	Before Cathodic Polarization	After Cathodic Polarization
Steel substrate			
0	0	2.2	3.2
10	90	4.1	6.7
20	80	15.0	29.7
30	70	29.0	39.6
100	0	74.3	85.8
Brass substrate			
0	0	2.1	3.2
10	90	3.9	6.8
20	80	15.4	30.7
30	70	35.2	47.0
100	0	148.7	130.9

It was pointed out by Boggio et al. [22] that the charge q^* can be used to monitor the stability of oxides electrodes. More specifically, stability is assumed to be excellent in case that q^* remained constant after an event occurred at the given electrode surface. If q^* decreases, this can be taken as due to loss of active material, even though it could even be due to smoothing of the electrode surface, which however appears unlikely, especially under H_2 or O_2 evolution. Thus, a small decrease in q^* observed with NiP-RuO_2 electrode on brass substrate, can be taken as an indication of loss of active material.

Hydrogen evolution in alkaline media is generally accepted to proceed via three steps. The mechanism involves initial proton discharge to form an adsorbed hydrogen atom on the metal surface, MH – Volmer reaction (Equation 1), followed by the electrochemical desorption of the hydrogen – Heyrovsky reaction (Equation 2) and/or the chemical desorption by the recombination of the adsorbed H atoms – Tafel reaction (Equation 3).

$$M + H_2O + e^- \Leftrightarrow MH + OH^- \quad (1)$$

$$MH + H_2O + e^- \Leftrightarrow H_2 + M + OH^- \quad (2)$$

$$MH + MH \Leftrightarrow H_2 + 2M \quad (3)$$

The electrocatalytic theory based on surface redox reactions allows to present a generalized mechanism for the main electrocatalytic reactions [23] where in a first step the surface is "prepared" by oxidation or reduction, while in successive steps the active sites interact with the reacting particles (H_2O, H^+ or OH^-) giving ultimately the product (O_2 or H_2). Clearly, a metal ion in an oxide differs from the same metal ion in the metal because of the environment in which it is "immersed". Thus, a certain metal ion is active in a metal, in an oxide or in a macrocycle matrix to a different degree depending on the "ligands". This very fundamental problem in electrocatalysis is also a reason why oxides are so investigated.

4. CONCLUSIONS

RuO_2/TiO_2 mixed oxide incorporated nickel-phosphorus coatings exhibited high electrocatalytic activity for HER. TiO_2 acted as an effective catalyst support for RuO_2.

Polarization curves recorded on mixed oxide reinforced NiP electrodes show a unique Tafel slope of approximately 120mV/dec in the whole potential range (–1.1/-1.5 V vs. SCE), while polarization curves obtained on NiP-RuO_2 composite coatings are bent with Tafel slopes of about 90 mV/dec at low current densities and 200 mV/dec at higher current densities. The curvature of the polarization curve can be explained by a bend towards a limiting current density at higher overpotenatials or by a change in reaction mechanism. The reaction rate on composite NiP-RuO_2/TiO_2 and NiP-RuO_2 is much faster (approximately 8-30 times) than on the plain Ni-P or NiP-TiO_2

composite electrode materials. NiP-RuO_2/TiO_2 electrode activity increases with RuO_2, thus NiP-RuO_2 electrode showing the highest activities on both types of substrates.

Measured volatammetric charges, q^* values increase with RuO_2 concentration increase as well as after cathodic hydrogen discharge, which suggests that the active surface has probably grown as a consequence of the solution spreading over regions made hydrophilic by the reductive treatment.

References

1. A. Lasia, Applications of the Electrochemical Impedance Spectroscopy to Hydrogen Adsorption, Evolution and Absorption into Metals. In: Conway BE, White RE, editors Modern Aspects of Electrochemistry, vol. 35. New York: Kluwer/Plenum, 2002. p. 1
2. S. Trasatti In: Gerischer H, Tobias CW. editors. Advances in electrochemical science and engineering, vol. 2. Weinheim, VCH, 1992. p. 2
3. S. Trasatti In: Wellington TC. editor. Modern chlor-alkali technology. Elsevier, Amsterdam, 1992. p. 281
4. E. R. KXotz, S. Stucki, *J. Appl. Electrochem.* 17 (1987) 1190
5. A. Lasia, A. Rami, *J. Electroanal. Chem.* 294 (1990) 123
6. J. P. Diard, B. Le Gorrec , S. Maximovich, *Electrochim. Acta*, 35 (1990) 1099
7. H. Chen, S. Trasatti, *J. Electroanal. Chem.* 357 (1993) 91
8. S.M.A. Shibli, V.S Dilimon, *Int. J. Hydrogen Energy*, 33 (2008) 1104-1111
9. S.M.A. Shibli, V.S Dilimon, *J. Solid State Electrochem.* 11 (2007) 1119-1126
10. S.M.A. Shibli, V.S Dilimon, *Int. J. Hydrogen Energy*, 32 (2007) 1694-1700
11. D. Gierlotka, E. Rowinski, A. Budniok, E. Lagiewka, *J. Appl. Electrochem.*27 (1997) 1349
12. S. Trasatti in J. Lipkowski, P.N. Ross (Eds.) The Electrochemistry of novel materials, VCH Pub., 1994, p.207
13. L.I. Krshtalik, *Electrochim. Acta*, 26 (1981) 329
14. A.C.C. Tseung, S. Jasem, *Electrochim. Acta*, 22 (1977) 31
15. S. Trasatti, "Physical Electrochemistry of Ceramic oxides", *Electrochim. Acta*, 36 (1991) 225
16. J. Novakovic and P. Vassiliou, *Electrochim. Acta* 54 (2009) 2499–2503
17. S. Ardizzone, S. Trasatti, *Adv. Colloid. Inerface. Sci.* 64 (1996) 173
18. A.Cornell, D, Simonsson, *J. Electrochem. Soc.* 140 (1993) 3123
19. S. Ardizzone, G. Fregonara, S. Trasatti, *Electrochim. Acta*, 35 (1990) 263
20. D. Baronetto, N. Krstajic, S. Trasatti, *Electrochim. Acta*, 39 (1994) 2359
21. S. Trasatti, *Electrochim. Acta*, 32 (1987) 369
22. R. Boggio, A Carugati, G. Lodi, S. Trasatti, *J. Appl. Electrochem.* 15 (1985) 335
23. S. Trasatti in H. Wendt (Ed.) Electrochemical Hydrogen Technologies, Elsevier, Amsterdam, 1985, p.1, 104